12th International Symposium on Turbulence and Shear Flow Phenomena (TSFP12)
Osaka, Japan, July 19–22, 2022

WAKE FLOW – ACOUSTIC RESONANCE IN A GENERIC AIR OUTLET

Asvath Ravichandran
Professorship of Hydromechanics
Technical University of Munich
Arccistr. 21, 80333 Munich, Germany
asvath.ravichandran@tum.de

Michael Manhart
Professorship of Hydromechanics
Technical University of Munich
Arccistr. 21, 80333 Munich, Germany
michael.manhart@tum.de

Florian Schwertfirm
Kreuzinger+ Manhart Turbulenz GmbH
Kirchenstr. 34, 81675 Munich, Germany
f.schwertfirm@km-turbulenz.de

Nikolaus Peller
HVAC Simulation
AUDI AG
Ingolstadt, Germany
nikolaus.peller@audi.de

ABSTRACT

We aim to investigate the noise generation mechanism in a generic geometry representing a typical air outlet of an HVAC system of a car. We use an Aero-Acoustic simulation based on Large-Eddy Simulation and an experiment to study the interaction between a throttle plate (used to control the flow rate) and fins (used to guide the flow). We can identify several sound generation mechanisms, of which the so-called Parker β-mode is the most prominent in the sensible frequency range. Our focus is on the interaction and resonance of this acoustic mode with the vortex shedding modes in the wake of the throttle valve, which seems to play a major role in determining the amplitude of the acoustic mode.

INTRODUCTION

The noise generated by the air outlet of the HVAC system of a car has attracted increasing research interest. The sources of noise generation in a HVAC unit can be classified into low frequency and high-frequency noises. The humming and buzzing noises at low frequency are mostly due to the components, namely blower and condenser. The tonal noises at high frequency are mostly from the air outlets, channels and discontinuities in the system such as air channel junctions. These are associated to the characteristic dimensions of the system namely duct height, section length and dimension of the flow guides (Perot et al., 2011). Guerin et al. (2005) have investigated the aero acoustics of an automotive air outlet with a generic model followed by different configurations namely, Throttle Valve (TV) parallel and inclined to the mean flow direction along with fins. When the TV was parallel to the flow direction only weak noise was observed with fins being the main noise source. But with the inclined TV, mutual interaction between the TV and fins resulted in a significant increase in broadband noise levels. It was seen that increasing the distance between TV and fins reduced the noise by several decibels. But this was observed only for the inclined TV configuration. The mutual interaction between TV and fins at different gap settings was not investigated for TV parallel to the mean flow direction.

From previous numerical and experimental investigations of flat plate, tandem plate and cascade plates (Hong et al., 2020; Stoneman et al., 1988; Parker, 1967; Koch, 2009; Yokoyama et al., 2013) an insight into the noise generation mechanisms of individual elements could be gained, but the interaction of those elements is still quite complex to interpret.

Previously, Kreuzinger et al. (2013) did a pure Computational Aero-Acoustic(CAA) simulation in an AUDI TT air outlet. It was concluded that the anti-symmetrical Parker's β-mode was not excited by the flow from the comparison with hybrid flow acoustic simulations and experiment. Also, Ravichandran et al. (2022) did investigations with different inflow conditions in an automotive series air outlet and a generic air outlet. The different inflow conditions had a slight effect on the increase in the amplitude of the resonance modes – particularly the β-mode – due to upstream turbulent intensity. The Parker-β-mode denotes the fundamental acoustic mode around the throttle valve with pressure oscillation in anti-phase above and below the center of the plate as proposed by Parker (1967). The pressure nodes and therefore anti-nodes of acoustic velocity are located at the leading edge and trailing edge of the throttle valve as in Ewert & Kreuzinger (2021) and Stoneman et al. (1988). The current paper considers the numerical results obtained to date, which are still a work in progress.

In this study, we investigate the reason for the strong excitation of the β-mode as the TV is moved closer to the fins, where a strong whistle noise is heard at a certain gap setting.

METHODOLOGY

We investigated a setup consisting of a test rig with a mass flow regulator, precursor channel and generic air outlet with microphone arrays in the far field as shown in Figure 1. The experimental setup of the generic air outlet is based on the work of Biermeier et al. (2012). The generic air outlet and the precursor channel are made of an acrylic glass (Figure 2). It also has a detachable as well as adjustable throttle valve and five fins for the investigation of aeroacoustic interaction as shown in the Figure 3. This setup has been exactly represented in the simulation. Its main parameters are given in Table 1.

Table 1. Computational and experimental parameters.

U_o (m s^{-1})	$Re_{Channel}$	$C_{l_1^*}/C_{t_1^*}$	$C_{l_2^*}/C_{t_2^*}$
25	8.49 x 10^4	25	10

Experiment

We performed a combined experimental/numerical study to investigate the effect of placing a throttle valve in front of the fins. The measurements were performed in a semi-anechoic chamber at AUDI. The setup has a precursor channel to achieve a fully developed flow. The precursor channel has a height $h = 0.05$ m, breadth $b = 0.05$ m and a length of $l = 10h$. The length of the TV was $C_{l_1^*} = h$ as sketched in the Figure 3. In this work, we investigate only at a gap setting of l_w=5C, where $C = C_{t_1^*} = C_{t_2^*}$.

Air is supplied by a blower unit integrated in a Valeo-Acoustic test rig (Figure 1). The noise generated by the blower is isolated with acoustic absorbing materials inside the settling chamber, which guarantees a low-noise inflow condition. The mass flow is supplied by a blower unit integrated in the test rig. The mass flow rate is calculated according to ISO 5801 via the pressure in the inflow nozzle.

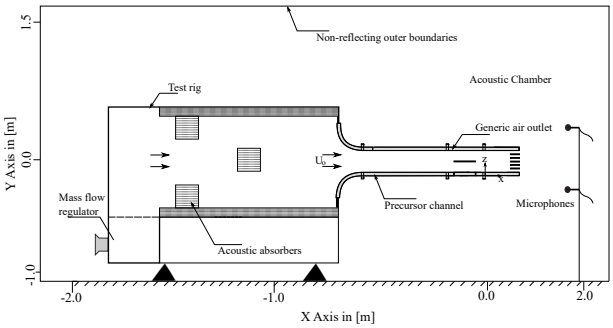

Figure 1. Schematic representation of the setup with far-field microphones

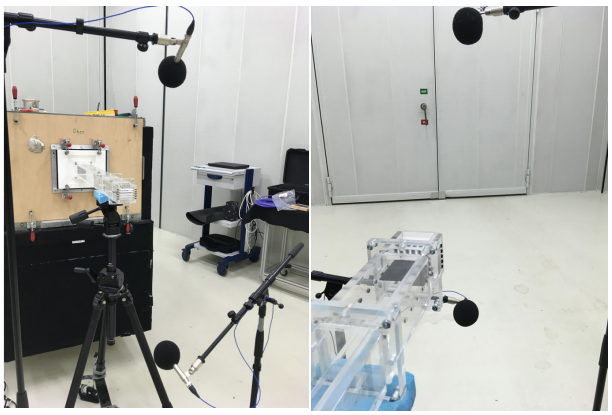

Figure 2. Experimental setup with the far-field microphones in a semi-anechoic chamber

Acoustic pressure signals were measured at the far-field microphones, visible in Figures 1 and 2. The microphones are placed at a distance of x=0.35 m from the air outlet centre at an angle of 45 degrees at -z and +z directions.

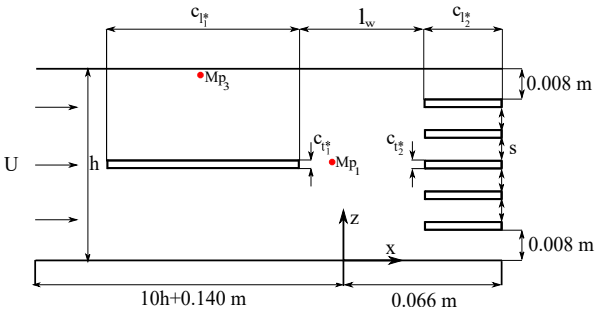

Figure 3. Sketch of the generic air outlet with Throttle Valve (TV) and fins in 2D along with the probe points Mp_1 and Mp_3

Numerical simulations

We used a hybrid approach to simulate the flow and the acoustic fields. The flow solver MGLET(Multi-Grid Large Eddy Turbulence) performs a wall-modelled Large Eddy Simulation using the WALE model proposed by Nicoud & Ducros (1999) with a wall function by Werner & Wengle (1993). MGLET is based on an Immersed Boundary Method (IBM) as described in Peller et al. (2006). The acoustic field is obtained by solving the Arbitrary Acoustic Perturbation Equation (APE) Ewert & Kreuzinger (2021) which is implemented in MGLET. The flow and acoustic simulations are performed on the same Cartesian grid, so no interpolations are necessary for the aero-acoustic source terms. The solver is a one way coupled solver with no feedback from the acoustics to the flow and has been validated by Schwertfirm et al. (2012).

In this hybrid CAA solver, the APE is solved with the following assumptions namely low mach number, an isentropic flow, neglecting the density gradients and the mean convection velocity. This leads to the following form of the APE

$$\frac{\partial u_i'}{\partial t} = -\frac{\partial p'}{\partial x_i} + \frac{1}{\rho_0}\frac{\partial p_{ic}}{\partial x_i} \tag{1}$$

and

$$\frac{\partial p'}{\partial t} = -\rho_0 c^2 \frac{\partial u_i'}{\partial x_i} \tag{2}$$

in which the source term p_{ic} is the incompressible or hydrodynamic pressure, taken from the incompressible flow solution. It can be shown that this set of equation is equivalent to solving a wave equation for the acoustic pressure p' in which the Laplacian of the incompressible pressure appears as a source term.

At the inflow boundary, a constant mass flux with a non-reflecting boundary for the acoustic pressure is set. At the outflow boundaries, Dirichlet conditions for either pressure or total pressure depending on flow direction and a Neumann condition for the velocities are used. A non-reflective boundary condition for the acoustic pressure and velocity is set at the outer boundaries of the domain. A global acoustic damping of 2% is set at the rigid walls.

The simulation domain has a size of (LX, LY, LZ)=(4,6 m, 2,6 m, 4,6 m). The generic air outlet is placed in the centre of the simulation domain. The grid has been constructed

of Cartesian grid blocks at 32^3 cubic cells, which are distributed among the CPU cores. A local refinement has been achieved by inserting locally refined grid boxes (Manhart, 2004). A grid resolution study was performed to determine the optimum compromise between accuracy and computational cost. This led to grid spacings of $\Delta x_{i,min}$=0.1875x10^{-3} m and $\Delta x_{i,max}$=12x10^{-3} m which were achieved by 6 refinement levels. In total 166002688 grid cells were used which were arranged in 5066 grid blocks. A time step of Δt=1.98x10^{-6} s kept the Courant-Friedrich-Lewy number below 0.5 and resulted in 200000 time steps for a sufficient flow statistics. This led to a computational time 98498.8 CPU hours using 1920 CPUs. The physical run time of simulation is t_{end}=0.5 s, sampling of statistics for flow and the acoustics field are started from 0.1 s. The physical parameters used are, density ρ= 1.165 kg m^{-3}, kinematic viscosity ν=1.53x10^{-5} m^2 s^{-1}.

VALIDATION

We performed a validation of the simulations by comparing with our experimental results. In Figure 4, we compare the measured pressure signal averaged over the microphone array with the correspondingly averaged total pressure signal of p' over the microphone array from the LES.

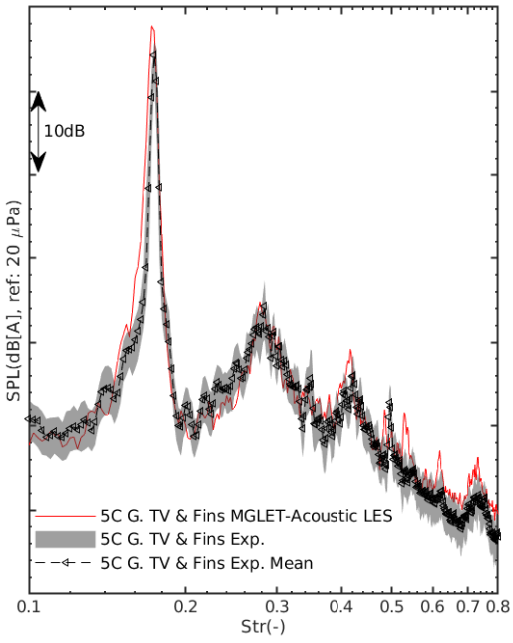

Figure 4. Validation of the acoustic simulation with experiment. Dimensionless Strouhal number Str=$\frac{f.C_{t_1^*}}{U_0}$, where U_0=25 m s^{-1} and $C_{t_1^*}$=0.002 m

The parameters used for the spectral calculations are as follows, a FFT with a Hann-window with 50% overlap, a sampling rate of 213441 Hz and a window width of 0.04 s was applied. This results in a frequency resolution of 25 Hz. The same FFT parameters were applied to the experimental data. As the measured time of the experimental data was around 20 s, the FFT was applied to the full signal (20 s) and to several shorter signal lengths around 0.4 s to increase the variance of experimental signal shown as grey band in the Figure 4 for a better comparability with the simulation signals.

The simulation predicts the experimental data up to a wide range of frequencies, and also most of the resonance peaks are well predicted by the simulation. The simulated spectrum lies within the variance of the experimental signal.

RESULTS AND DISCUSSION

In this section, the vortex shedding behind the throttle valve and the acoustic resonance mode on the throttle valve will be further investigated with the simulation results.

The noise generation of different elements, for a gap setting of l_w=5C, $C = C_{t_1^*} = C_{t_2^*}$ is shown in Figure 5. The configuration without elements '5C G. Channel' has no distinct peak at any Strouhal number and generally a low noise level. Inserting the throttle valve (configuration '5C G. TV') leads to an increased noise level with a clear peak at a Strouhal number (Str=0.1799) which can be assigned to Parker's β-mode, which is explained in the next sections. Further adding the fins (configuration '5C G. TV & Fins'), the noise level close to this frequency is strongly enhanced while it remains low with the fins only. This lets us conclude that the interaction between fins and TV generates this enhanced noise level due to an interaction between the elements.

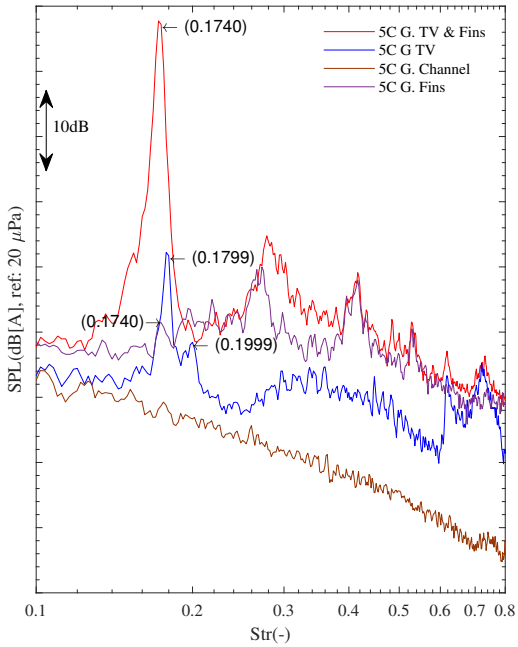

Figure 5. The noise generation of different elements, shown, is the Sound Pressure Level (SPL) of total pressure $p' = P_a + P_{ic}$ at far-field microphones. Dimensionless Strouhal number(Str)=$\frac{f.C_{t_1^*}}{U_0}$, where U_0=25 m s^{-1} and $C_{t_1^*}$=0.002 m

In Figure 6 a snapshot of the instantaneous u-component of the flow around the fins is shown for the configuration with throttle valve and fins. The vortex shedding behind the throttle valve can be clearly seen. This flow field emits acoustic waves, as seen in Figure 7, in which the acoustic pressure p' is rendered in the total computational domain.

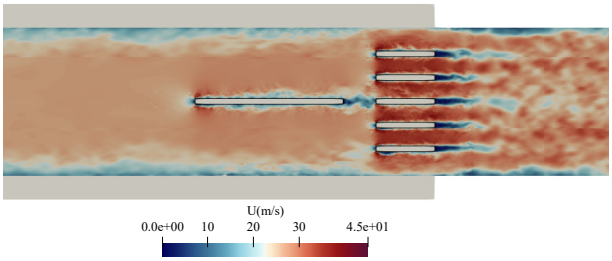

Figure 6. Instantaneous flow field U of '5C G. TV & Fins' configuration

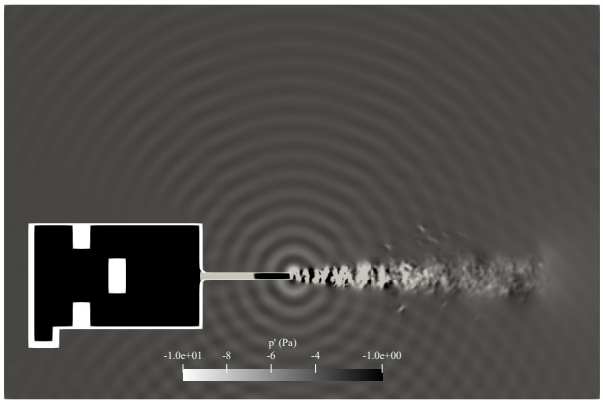

Figure 7. Simulation: Instantaneous total pressure $p' = P_a + P_{ic}$ of configuration '5C G. TV & Fins', showing ground reflections and also the dipole characteristics of Parker β-mode

Previously, Biermeier et al. (2012) investigated the Parker β mode for different plate lengths starting from $C_{l_1^*}$=0.0208 to 0.0404 m and compared the measured values with the Parker mode diagram. The same Parker mode diagram, with four simplest modes is shown in Figure 8. The diagram is generated using the MATLAB script taken from the thesis work of Tautz (2012). From the Parker mode diagram, the resonant frequency value for the β-mode for the throttle valve and channel in our case can be calculated.

The peak (Str=0.1799) in the '5C G. TV' spectrum corresponds to f=2249 Hz. This frequency f is taken for the calculation of Parker's non-dimensional resonance frequency f^*. The non-dimensional resonance frequency of $f^* = \frac{f.d_0}{c} = 0.3174$ and with non-dimensional plate length of $l^* = \frac{C_{l_1^*}}{d_0\sqrt{1-Ma^2}} = 1.046$ corresponds to the β-mode as in Parker (1967) and corresponding to Koch (2009) calculation scheme, where $d_0 = h - C_{t_1^*}$, speed of sound c=343 m s^{-1} and Mach number Ma=0.07288. The results are plotted in the Figure 8, where in simulation f=2249 Hz and the theoretical value of β-mode at f=2255 Hz with a deviation of only Δf= 6 Hz. The shift of the other peak (Str=0.1740) in '5C G. TV & Fins' is further discussed.

We are further analysing the probe points Mp_1 and Mp_3 to understand the frequency related to vortex shedding and the β-mode, where Mp_1 is placed in the wake of the TV and Mp_3 is at the centre of the duct close to the wall as shown in the Figure 3. The further analysis is performed with the two configurations, namely '5C G.TV' and '5C G. TV & Fins'. The reason for chosen configurations above is to understand how the fins in the air outlet change the flow-acoustic interaction.

The peaks at the far-field are correlated to the peaks at

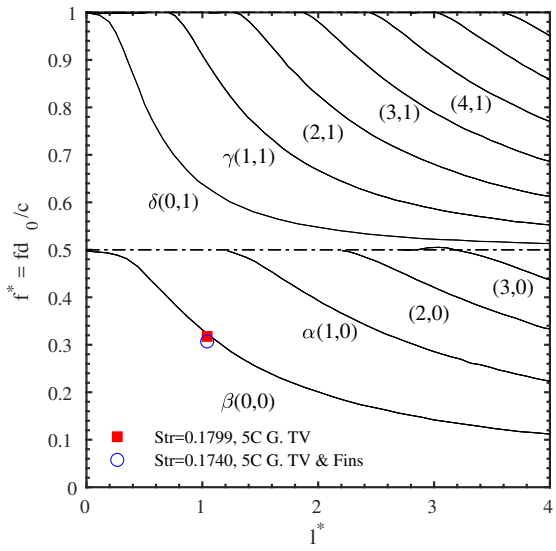

Figure 8. Parker mode diagram, x-axis corresponds to the non- dimensional plate length l^* and y-axis corresponds to the non-dimensional resonance frequency f^*

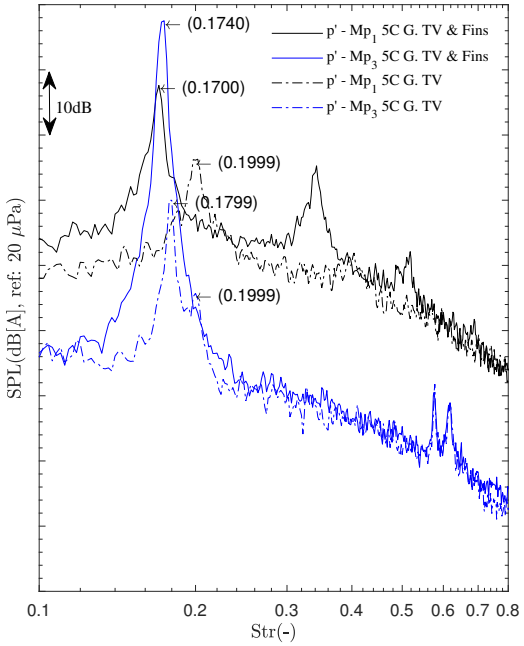

Figure 9. Sound Pressure Level (SPL) of total pressure $p' = P_a + P_{ic}$ at microphone probes as shown in the sketch.

the probe points inside the generic air outlet. In the Figure 9, An interesting observation is in the '5C G. TV' configuration that the peak (Str=0.1799) at the far field p' coincides exactly with the probe point 'p'- Mp$_3$ 5C G.TV' at the duct wall above the throttle valve. The other peak(Str=0.1999) at the far field p' coincides exactly with the probe point 'p'-Mp$_1$ 5C G. TV' behind the wake of the throttle valve. The latter peak (Str=0.1999) can be the trace of the vortex shedding in the wake of the throttle valve.

Whereas in '5C G. TV & Fins', the peak (Str=0.1740)

at the far field p' coincides exactly with the probe point 'p'-Mp_3 5C G.TV & Fins' at the duct wall above the TV. The peak (Str=0.1700) at the probe point 'p'- Mp_1 5C G.TV & Fins' is close to the far field peak, It looks like the vortex shedding frequency shifted to low frequency due to addition of fins. For the further investigation, the incompressible flow field and the acoustic components are treated separately. The hydrodynamic pressure P_{ic}, which is the result of the incompressible flow solver, and the acoustic pressure P_a, which is computed from the solution p' of the APE and the solution p_{ic} of the incompressible Navier-Stokes equations. At the microphone signal in simulation, the incompressible or hydrodynamic pressure P_{ic} and acoustic pressure P_a can be separated. The spectrum of respective pressure P_{ic} and P_a at the probe points Mp_1 and Mp_3 are shown in the Figures 10 and 11.

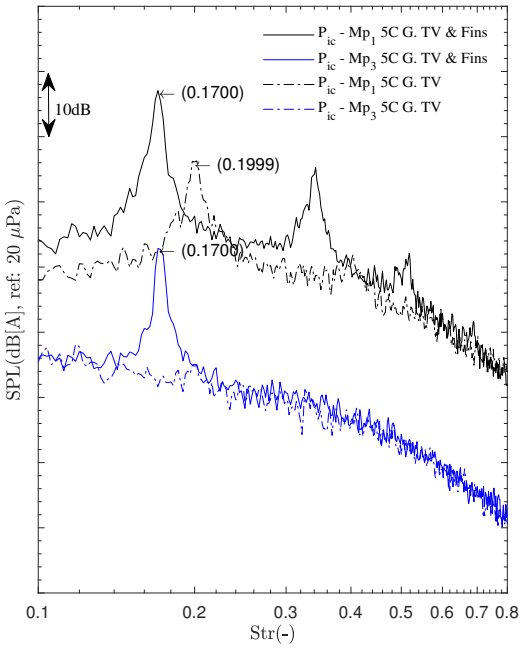

Figure 10. Sound Pressure Level (SPL) of incompressible hydrodynamic pressure P_{ic} at microphone probes, as shown in the sketch.

From the Figure 10, The incompressible pressure shows that the peak(Str=0.1999) at 'P_{ic}-Mp_1 5C G. TV' behind the wake is a hydrodynamic mode. This let us conclude that this is a vortex shedding mode. In 'P_{ic}-Mp_1 5C G. TV & Fins' looking at the hydrodynamic pressure, the vortex shedding mode shifts to a slightly low frequency(Str=0.1700) due to the addition of the fins.

Further, analysing from the figure 11, the acoustic spectrum at the probe points 'Mp_1' and 'Mp_3' for both configurations '5C G.TV' and '5C G.TV & Fins' are shown. The amplitude of Sound Pressure Level is higher at the probe point 'Mp_3' than 'Mp_1' in the wake for both of the configurations, showing that the geometric Parker-β mode is dominant. The trace of the vortex shedding noise is also noticeable in the spectrum. It can be observed that the consecutive peaks at Str=0.1799 and Str=0.1999 in the configuration '5C G.TV' has a ΔStr=0.02. Whereas in the configuration '5C G.TV & Fins', the trace of vortex shedding frequency at Str=0.1700 is very close to the Parker-β mode frequency at Str=0.1740 for the TV. These two oscillators, oscillating close to the same frequency with a ΔStr=0.004 gets enhanced with noise levels at this particular spacing. It is also quite not so clear why the geometric Parker-β mode in the acoustic pressure spectrum shifted from Str=0.1799 to Str=0.1740 after adding fins closer to the throttle valve.

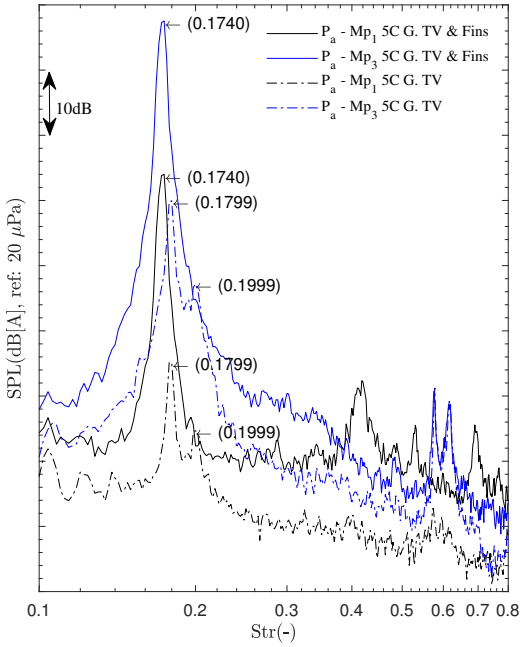

Figure 11. Sound Pressure Level (SPL) of acoustic pressure P_a at microphone probes as shown in the sketch.

In the simulation, a more detailed information on the observed peaks are gained by doing a Fourier Transformation (FT) of the acoustic pressure P_a and hydrodynamic pressure P_{ic} at selected frequencies during run time of the simulation. For the method of In-Situ-FT used here, please refer to Kreuzinger et al. (2013). For the two configurations with and without fins, the In-Situ-FT has been carried out for selected frequencies. The In-Situ-FT pictures of acoustic pressure P_a and hydrodynamic pressure P_{ic} of configurations with and without fins along with throttle valve are shown in the Figure 12. The acoustic and hydrodynamic pressure are scaled with same SPL values for a fair comparison. The reason for the increase in the amplitude at Str=0.1740 in the p' spectrum will be discussed with the insitu-FT modes. The amplitude of the modes in the '5C G. TV' configuration is quite low, of which the β-mode in Figure 12(a) and vortex shedding mode in Figure 12(b) are not oscillating close to a single frequency. Whereas in the '5C G. TV & Fins' configuration, the vortex shedding mode got intensified due to addition of fins in Figure 12(d) very close to the Parker β-mode frequency in Figure 12(c), these two oscillators at very close frequency resulted in increase in amplitude of the acoustic mode.

Conclusion

The hybrid CAA method used here can predict the resonance frequencies, which is quite in good agreement with the

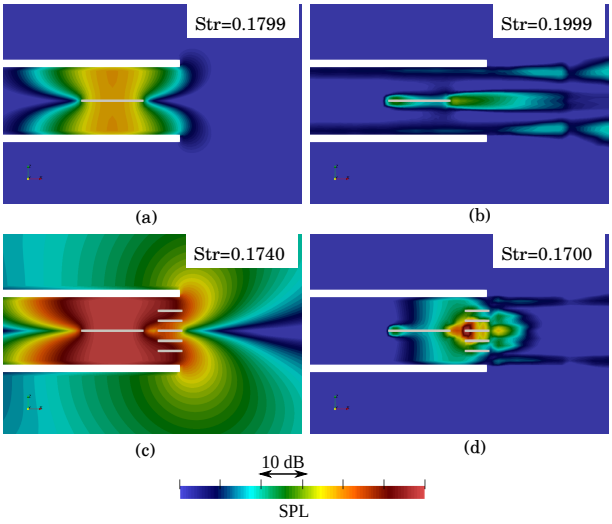

Figure 12. Insitu-FT of (a) P_a-'5C G. TV', (b) P_{ic}-'5C G. TV', (c) P_a-'5C G. TV & Fins', (d) P_{ic}-'5C G. TV & Fins'.

experimental observations. From the numerical observations, the hydrodynamic and acoustic modes can be treated separately to differentiate the modes related to flow and acoustics, which has given further insights on this interaction. The enhanced amplitude of the β-mode is due to the vortex shedding at the matching frequency. This phenomenon can be captured with one-way flow acoustic coupling, as there is no feedback from acoustic to flow required in this particular case.

Acknowledgement

The first author wishes to acknowledge the support from AUDI AG in cooperation with TUM under INI.TUM program. The authors acknowledge the support of technicians of TUM's Hydromechanic lab for constructing the generic air outlet and AUDI AG for providing the acoustic chamber and hot-wire measurement facilities.

REFERENCES

Biermeier, Thomas, Becker, Stefan & Risch, Paul 2012 Acoustic investigations of hvac systems in vehicle. Tech. Rep.. SAE Technical Paper.

Ewert, Roland & Kreuzinger, Johannes 2021 Hydrodynamic/acoustic splitting approach with flow-acoustic feedback for universal subsonic noise computation. Journal of Computational Physics **444**, 110548.

Guerin, S, Thomy, E & Wright, MCM 2005 Aeroacoustics of automotive vents. Journal of sound and vibration **285** (4-5), 859–875.

Hong, Zhiliang, Wang, Xiaoyu, Jing, Xiaodong & Sun, Xiaofeng 2020 Vortex sound interaction in acoustic resonance of a flow duct containing a plate. Journal of Sound and Vibration **483**, 115482.

Koch, Werner 2009 Acoustic resonances and trapped modes in annular plate cascades. Journal of fluid mechanics **628**, 155–180.

Kreuzinger, Johannes, Schwertfirm, Florian, Hartmann, Michael & Peller, Nikolaus 2013 Analysis of resonance phenomena caused by obstacles in hvac exhaust nozzles using a combined cfd-caa approach. In 19th AIAA/CEAS Aeroacoustics Conference, p. 2132.

Manhart, M. 2004 A zonal grid algorithm for DNS of turbulent boundary layers. Computers and Fluids **33** (3), 435–461.

Nicoud, Franck & Ducros, Frédéric 1999 Subgrid-scale stress modelling based on the square of the velocity gradient tensor. Flow, turbulence and Combustion **62** (3), 183–200.

Parker, R 1967 Resonance effects in wake shedding from parallel plates: calculation of resonant frequencies. Journal of Sound and Vibration **5** (2), 330–343.

Peller, Nikolaus, Duc, Anne Le, Tremblay, Frédéric & Manhart, Michael 2006 High-order stable interpolations for immersed boundary methods. International Journal for Numerical Methods in Fluids **52** (11), 1175–1193.

Perot, Franck, Meskine, Mohammed, Vergne, Sandrine & Gille, Frederic 2011 Aeroacoustics prediction of simplified and production automotive hvac ducts and registers. In 17th AIAA/CEAS Aeroacoustics Conference (32nd AIAA Aeroacoustics Conference), p. 2935.

Ravichandran, Asvath, Logdesser, Andreas, Peller, Nikolaus & Manhart, Michael 2022 Experimentelle und numerische untersuchung des effekts der zuströmbedingungen auf die schallabstrahlung eines generischen ausströmers. In DAGA 2022 - 48. Jahrestagung fr Akustik, pp. 1250–1253.

Schwertfirm, Florian, Kreuzinger, Johannes, Peller, Nikolaus & Hartmann, Michael 2012 Validation of a hybrid simulation method for flow noise prediction. In 18th AIAA/CEAS Aeroacoustics Conference (33rd AIAA Aeroacoustics Conference), p. 2192.

Stoneman, SAT, Hourigan, K, Stokes, AN & Welsh, MC 1988 Resonant sound caused by flow past two plates in tandem in a duct. Journal of Fluid Mechanics **192**, 455–484.

Tautz, Matthias 2012 Fluid-akustik interaktion bei der umströmung von platten in kan"alen. PhD thesis, Diplomarbeit am Lehrstuhl fr Prozessmaschinen und Anlagentechnik der Friedrich-Alexander-Universität Erlangen-Nürnberg.

Werner, H & Wengle, H 1993 Large-eddy simulation of turbulent flow over and around a cube in a plate channel. In Turbulent shear flows 8, pp. 155–168. Springer.

Yokoyama, H, Kitamiya, K & Iida, A 2013 Flows around a cascade of flat plates with acoustic resonance. Physics of Fluids **25** (10), 106104.